First Experimental Observation of Superscars in a Pseudointegrable Barrier Billiard

E. Bogomolny,[1] B. Dietz,[2] T. Friedrich,[2] M. Miski-Oglu,[2] A. Richter,[2,*] F. Schäfer,[2] and C. Schmit[1]

[1]*Laboratoire de Physique Théorique et Modèles Statistiques, Université de Paris-Sud, Bâtiment 100, 91405 Orsay Cedex, France*

[2]*Institut für Kernphysik, Technische Universität Darmstadt, D-64289 Darmstadt, Germany*

(Received 17 August 2006; published 20 December 2006)

With a perturbation body technique intensity distributions of the electric field strength in a flat microwave billiard with a barrier inside up to mode numbers as large as about 700 were measured. A method for the reconstruction of the amplitudes and phases of the electric field strength from those intensity distributions has been developed. Recently predicted superscars have been identified experimentally and—using the well-known analogy between the electric field strength and the quantum mechanical wave function in a two-dimensional microwave billiard—their properties determined.

DOI: 10.1103/PhysRevLett.97.254102 PACS numbers: 05.45.Mt, 03.65.Sq, 42.25.Fx

Planar polygonal billiards with angles $\alpha_j = \pi m_j/n_j$, where m_j and n_j are coprime integers, have been studied both classically and quantum mechanically [1]. When $m_j \neq 1$ the motion in phase space is not restricted to a torus like for integrable systems, but to a surface with a more complicated topology. Accordingly, such planar polygonal billiards are called pseudointegrable. It was established numerically (see [2,3] and references therein) that the statistical properties of the eigenvalues of the corresponding quantum systems are intermediate between those of a regular and a chaotic system. The properties of the wave functions of planar polygonal billiards are also intriguing, as they show a strong scarring behavior which can be related to families of periodic orbits [4]. In a plot of eigenfunctions in the barrier billiard scars are clearly distinguishable from nonscarred eigenfunctions. This pronounced scar structure does not disappear at large quantum numbers in contrast to that in chaotic systems [5–7]. To stress this difference it is proposed in [4] to call the scars in pseudointegrable systems superscars, an expression used by Heller in his early seminal Letter [6] in a different context. The aim of this Letter is to report on the experimental investigation of superscars in the barrier billiard. This is a rectangular billiard of area $l_x \cdot l_y$ which contains an infinitely thin barrier. In the experiment presented here, the barrier is placed on the symmetry line $x = l_x/2$ and its length equals $l_y/2$, where l_y is the length of the shorter side of the rectangle.

In the present work the quantum barrier billiard is simulated by means of a microwave billiard. Microwave billiards are flat cylindrical resonators [8,9]. Below the critical frequency $f_c = c/2h$, where c is the velocity of light and h is the height of the cavity, the electric field is the solution of the scalar Helmholtz equation with Dirichlet boundary conditions. This equation is mathematically equivalent to the Schrödinger equation for a quantum billiard of corresponding shape (see, e.g., [8,9]).

The experimental observation of the superscars predicted in [4] requires (i) the detection of eigenmodes at sufficiently high quantum numbers N and (ii) the resolution of all modes up to these quantum numbers. The number $N(f_c)$ of resonances below the critical frequency f_c is approximately given by the first term of the Weyl formula [10], i.e., $N(f_c) = \frac{A}{4\pi}(\frac{2\pi}{c} f_c)^2 = \frac{A}{4\pi}(\frac{\pi}{h})^2$, where A is the area of the billiard. Hence, the number of experimentally accessible resonances increases with the area and decreases with the height of the billiard. The resonances can be well resolved, if their widths are small in comparison with the average spacing between adjacent resonances, i.e., a microwave cavity with a high quality factor Q is needed. The latter is proportional to the ratio of the volume to the surface of the cavity, therefore, for flat cylindrical resonators to the height of the resonator. A compromise between a high Q and a large number of resonances is obtained by designing a rectangular cavity with side lengths of $l_x = 1000$ mm and $l_y = 585$ mm, and a height of $h = 25$ mm. The barrier has length 297 mm, a width of 4 mm, and the same height as the rectangular cavity. As in our earlier experiments [11] the resonator consists of a bottom, a lid, and a frame in between. All parts are squeezed together with screws. The bottom and lid plates, respectively, are manufactured from polished copper. The frame has the shape of a rectangle and consists of 10 brass segments. To ensure a proper electrical contact even at high frequencies, wires of solder are placed between the bottom, the frame, and the lid. The so constructed microwave barrier billiard has about 700 resonances below $f_c = 6$ GHz, the average quality factor is $Q = 1.8 \times 10^4$, and the mean resonance width is at least 10 times smaller than the mean resonance spacing.

In order to obtain information on the wave functions in the quantum barrier billiard we determined the electric field strength distribution in the corresponding microwave billiard. Thus first intensity distributions of the electric field strength were measured with the so-called perturbation body method [12]. A small metallic body alters the resonance frequency f_0 of the cavity, where according to the Maier-Slater theorem [13] the frequency shift depends

on the difference of the squares of the electric field strength E and the magnetic field B at its location inside the cavity:

$$\Delta f = f_0(c_1 E^2 - c_2 B^2). \quad (1)$$

Here, c_1 and c_2 are constants determined by the geometry and material of the perturbation body. In order to obtain the electric field strength distribution, the perturber needs to be moved inside the closed resonator. This is best done with an external guiding magnet. However, since we are interested in the electric field strength only, the magnetic field contribution in Eq. (1) has to be removed. In earlier experiments [12,14–16] with microwave billiards the magnetic field contribution to the frequency shift was minimized by using a needlelike metallic bead. We, for the first time, used a *nonmetallic* perturber (of so-called magnetic rubber) which is a rubberlike plastic combined with barium ferrite powder, whose grain size is of the same order of magnitude (1–10 μm) as the skin depth of radio frequency waves. Therefore, eddy currents cannot propagate, such that the magnetic rubber does not interact with the microwave magnetic field B. Accordingly there is no contribution to Δf in Eq. (1).

We first performed test measurements with the rectangular cavity and a cylindrical perturbation body with a height of 5 mm and a diameter of 2 mm. Typically the positive frequency shift induced by the electric field strength is of the order of 100 kHz. As expected, we did not detect any negative frequency shifts, which would result from the magnetic field term in Eq. (1) within the experimental uncertainty of the frequency shift measurement of about 1 kHz. Moving the perturbation body with an external guiding magnet across the billiard surface with a spatial resolution of about one-tenth of a wavelength and measuring the frequency shifts Δf at each of its positions yields the intensity distribution of the electric field strength in the whole microwave billiard. The shift Δf is determined as in [17] via phase shift measurements. In the frequency list mode the vectorial network analyzer HP8510C allowed the simultaneous measurement of the phases at up to 30 different frequencies. This enabled us to crucially reduce the measurement time; we measure 30 intensity distributions in one raster scan for a grid with 200×100 points in 12 hours. To minimize the influence of a temperature drift, which causes an additional frequency shift of about 40 kHz/K, the temperature of the microwave billiard was stabilized to within 0.1 K.

Because of the symmetry of the barrier billiard there are two types of modes, antisymmetric and symmetric ones with respect to the symmetry line defined by the barrier, respectively. The former are trivial as they coincide with those of the rectangular billiard; the latter are exactly those in which we are interested. We were able to measure, with the advanced experimental method described above, the intensity distributions of altogether 590 modes for level numbers $N = 90$–680. In contrast to the technique described in [18] with the perturbation body method we detect the E field intensity only. For a detailed investigation of the symmetric mode properties we developed a special procedure to reconstruct the E field, i.e., the quantum mechanical wave function ψ, itself and its sign from the measured intensity distribution.

For this we fit the square of a sine series to the measured field intensity. Along a line of constant x, $x = x_0$, in the billiard plane the latter can be represented as

$$\psi_k^2(x = x_0, y) = \left[\sum_{i=1}^{n} A_i(x_0) \sin k_i y\right]^2, \quad (2)$$

where $k_i = \pi i / l_y$, l_y is the length of the billiard along the line $x = x_0$, and $A_i(x_0)$ are the expansion coefficients. With this choice of k_i the Dirichlet boundary condition is automatically fulfilled. The number of terms giving a significant contribution to the sum can be estimated semiclassically, i.e., $n \sim 2l_y/\lambda$ and $\lambda = 2\pi/k$. For the determination of the expansion coefficients $A_i(x_0)$ in Eq. (2) a nonlinear fit routine which is based on the Levenberg-Marquardt algorithm [19] was used. The nonlinear fit requires a trial vector of coefficients as initial values. We used random numbers which are uniformly distributed in the interval from $-\max(|\psi(x = x_0, y)|)$ to $\max(|\psi(x = x_0, y)|)$ as entries of the trial vector, whose typical dimension is about $n = 20$. The nonlinear fit has no unique solution as the Levenberg-Marquardt algorithm only provides a set of coefficients $A_i(x_0)$ which gives a local minimum in χ^2. To find the global minimum we generated about 1000 trial vectors and carried out a fit for each of these. Then that set of coefficients $A_i(x_0)$, which gives the smallest χ^2, provides the wave function values along the line with constant $x = x_0$. Because of the continuity of the wave function for the neighboring lines we can use the so determined coefficients as entries of their trial vectors. An example for the measured intensity and the reconstructed field of the eigenmode with $N = 613$ and frequency $f = 5.48004$ GHz is shown, respectively, in Fig. 1. From 290 measured intensity distributions corresponding to the symmetric wave functions we reconstructed 230. For the remaining 60 distributions, due to large noise or nearly overlapping resonances, reconstruction was not possible.

Among the large number of wave functions several superscarring ones were observed. Four examples of de-

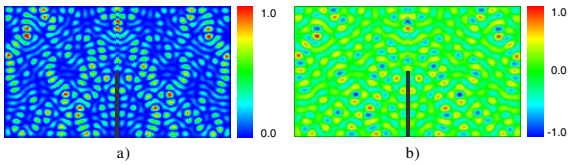

FIG. 1 (color online). (a) The measured intensity distribution for the mode $N = 613$. (b) The reconstructed E field, i.e., the wave function. The corresponding color scales are in the right-hand side of the graphs.

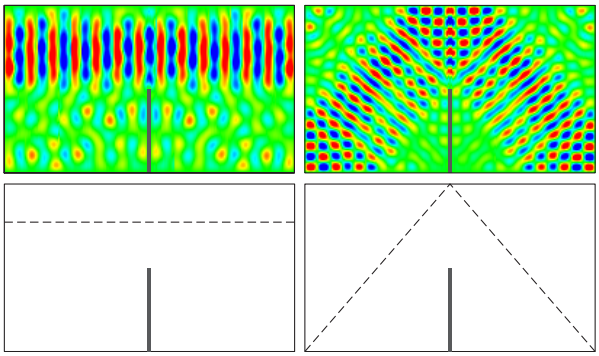

FIG. 2 (color online). The top row shows examples of experimentally obtained superscars in the barrier billiard. The color scale is the same as in Fig. 1(b). In the bottom row the corresponding classical orbits are indicated (dashed lines).

tected superscars are shown in Figs. 2 and 3. Each wave function shows a clear structure which is obviously related to the corresponding periodic orbit (PO).

To understand the quantum nature of the superscars we briefly outline how the PO families of a barrier billiard can be constructed. For this purpose we mark one corner of the barrier billiard with a black point as shown in Fig. 4(a), thus defining the initial orientation of the billiard. We follow the orbit of the propagating particle [dashed line in Fig. 4(a)] and mirror the billiard each time the particle hits a side of the billiard. This procedure is repeated until the mirrored copy of the billiard resumes its initial orientation. All parallel trajectories with the same length form a family of POs. Each family corresponds to an infinitely long periodic orbit channel (POC). This POC is confined to the region between the two straight lines which connect the singularities, i.e., the barrier tip and its images. These lines are called the singular diagonals (SD). In the semiclassical limit we can associate with each classical trajectory a wave. Waves traveling in a POC are scattered at an infinite array of images of the barrier tip. At the SD the intensity of the scattered wave is proportional to $1/\sqrt{k}$, where k is the wave momentum [20]. Therefore, it tends to zero and fulfills the Dirichlet boundary condition there with increasing k. Accordingly, in the semiclassical limit the SD act as perfect mirrors such that in each POC quasistates can be constructed. These are called unfolded scar states in [4] and are given as

$$\Psi^{\mathrm{scar}}_{m,n}(\xi,\eta) = e^{-ik_m\xi}\sin\left(\frac{\pi n}{w}\eta\right)\chi(\eta). \tag{3}$$

Here ξ is the coordinate along the POC and η ($0 < \eta < w$) the one perpendicular to it, and w is the channel width. The quantity $\chi(\eta)$ is the characteristic function of the POC [$\chi(\eta) = 1$ if $0 < \eta < w$, and $\chi(\eta) = 0$ otherwise]. The frequency of the eigenfunction [Eq. (3)] of the POC is

$$f_{m,n} = \frac{c}{2\pi}\sqrt{k_m^2 + \left(\frac{\pi n}{w}\right)^2}. \tag{4}$$

Because of the Dirichlet boundary condition the wave gains a phase of π each time the classical trajectory crosses the billiard boundary. If the PO experiences an even number of boundary crossings while traveling through the POC, then $k_m = 2\pi m/l$, otherwise $k_m = \pi(2m+1)/l$, where l is the length of the PO. When folding back the unfolded superscar states of Eq. (3), complicated expressions for folded scar states $\Psi_{m,n}(x,y)$ are obtained which, except on the SD, obey the Schrödinger equation for the barrier billiard $[\Delta + (\frac{2\pi}{c}f_{m,n})^2]\Psi_{m,n}(x,y) = 0$ with Dirichlet boundary conditions on the billiard boundary. As can be seen in Fig. 4(b) the experimentally obtained superscarring wave functions are mainly concentrated inside the corresponding POC. This confirms the approximate validity of the ansatz for the superscar wave functions given in Eq. (3).

A typical eigenfunction of the barrier billiard may have contributions from many scar states. In order to obtain a quantitative measure for this we followed Ref. [4] and computed the overlap integral of folded scar states $\Psi^{\mathrm{scar}}_{m,n}(x,y)$ given in Eq. (3) with the measured wave function $\Psi_{\tilde{f}_\lambda}(x,y)$ at the unfolded resonance frequencies $\tilde{f}_\lambda$,

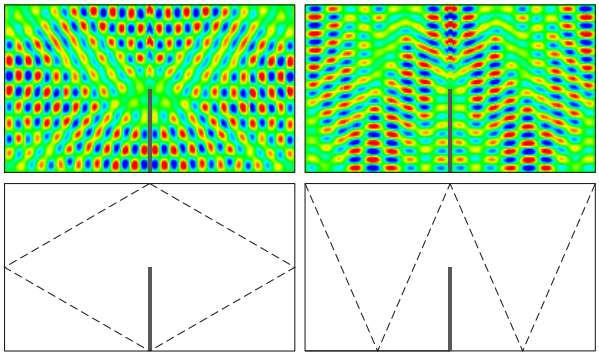

FIG. 3 (color online). The same as in Fig. 2 but for two other types of superscars.

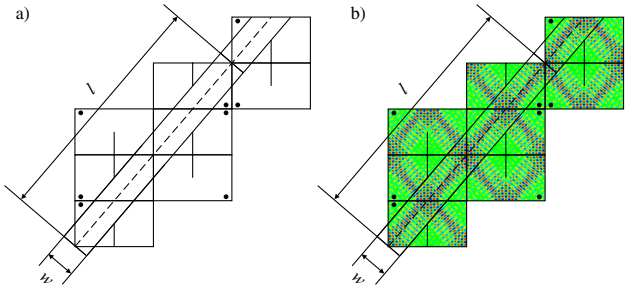

FIG. 4 (color online). (a) Illustration of the construction of the PO channel. The black point in the upper left corner of the original billiard fixes its initial orientation. (b) The unfolding of the experimentally obtained superscarring wave function with number $N = 587$. It has 110 wave maxima along the POC and one perpendicular to it, corresponding to the quantum numbers $m = 55$ and $n = 1$, respectively.

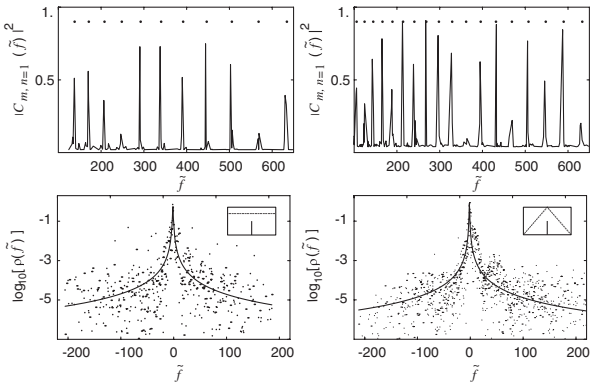

FIG. 5. The top row shows the overlap of measured wave functions of the barrier billiard with analytically constructed scar states for different POs. The points indicate the predicted positions of the superscar at the rescaled frequency $\tilde{f}$. In the bottom row the corresponding local density is plotted. The solid lines indicate the best fit of a Breit-Wigner shape to the data. The insets show the corresponding PO families.

where the unfolding was performed as usual [8,9] using the Weyl formula [10],

$$C_{m,n}(\tilde{f}_\lambda) = \int \Psi^{\mathrm{scar}}_{m,n}(x,y)\Psi_{\tilde{f}_\lambda}(x,y)dxdy. \qquad (5)$$

In the computations we fixed the number of excitations perpendicular to the POC to $n = 1$; m is obtained from the condition that $|\tilde{f}_\lambda - \tilde{f}_{m,n}|$ should be minimal. The resulting squares of overlap coefficients $|C_{m,n}(\tilde{f})|^2$, versus the unfolded resonance frequency $\tilde{f}$ for two different families of superscars, are shown in Fig. 5. The frequencies of the superscars are given by Eq. (4). Near almost all predicted superscar frequencies, marked by points in Fig. 5, we found a wave function with a strong contribution to the integral of overlap with a constructed superscar state.

To analyze the overlap of the constructed superscars with the neighboring nonscarred states, we calculated the average over all the spikes showed in Fig. 5, and obtained the so-called local density of states averaged over different m,

$$\rho_n(\tilde{f}) = \left\langle \sum_\lambda |C_{m,n}(\tilde{f}_\lambda)|^2 \delta(\tilde{f} - \tilde{f}_\lambda + \tilde{f}_{m,n}) \right\rangle_m . \qquad (6)$$

In the bottom row of Fig. 5 this quantity is shown for the two scar families in the top row of the figure. It is evident that the constructed superscars Eq. (3) have a certain overlap with the neighboring states. The finite width of the local density curves indicates that the Dirichlet boundary condition along the SD is an approximation, that is, the field can leak out of the POC. As can be seen in Fig. 5, it seems to be reasonable to approximate the averaged local density of the superscar states by a Breit-Wigner shape, but further work on this is in progress.

In summary, we have measured the electric field strength distributions at 590 resonance frequencies of the barrier billiard and reconstructed almost all corresponding symmetric wave functions. Many of the wave functions show a surprisingly pronounced structure of so-called superscars which is connected with classical PO families. We plan to extend our measurements of wave functions in barrier billiards with one or more nonsymmetrically placed barriers. The statistical properties of the nodal domains of polygonal billiards are another very interesting problem, which will be investigated.

This work has been supported within the DFG Grant No. SFB634.

*Electronic address: richter@ikp.tu-darmstadt.de

[1] P. J. Richens and M. V. Berry, Physica (Amsterdam) **2D**, 495 (1981).
[2] E. Bogomolny, U. Gerald, and C. Schmit, Phys. Rev. E **59**, R1315 (1999).
[3] J. Wiersig, Phys. Rev. E **65**, 046217 (2002).
[4] E. Bogomolny and C. Schmit, Phys. Rev. Lett. **92**, 244102 (2004).
[5] S. W. McDonald, Lawrence Berkeley Laboratory Report No. LBL-14837, 1983 (unpublished).
[6] E. J. Heller, Phys. Rev. Lett. **53**, 1515 (1984).
[7] T. M. Antonsen *et al.* Phys. Rev. E **51**, 111 (1995).
[8] H.-J. Stöckmann, *Quantum Chaos: An Introduction* (Cambridge University Press, Cambridge, England, 2000).
[9] A. Richter, in *Emerging Applications of Number Theory*, edited by D. A. Hejhal, J. Friedmann, M. C. Gutzwiller, and A. M. Odlyzko, The IMA Volumes in Mathematics and Its Applications Vol. 109 (Springer, New York, 1999), pp. 479–523.
[10] H. Weyl, Journal für die reine und angewandte Mathematik **141**, 1 (1912).
[11] C. Dembowski *et al.* Phys. Rev. E **62**, R4516 (2000); Phys. Rev. Lett. **93**, 134102 (2004).
[12] S. Sridhar, D. Hogenboom, and B. Willemsen, J. Stat. Phys. **68**, 239 (1992).
[13] L. C. Maier, Jr. and J. C. Slater, J. Appl. Phys. **23**, 68 (1952).
[14] A. Gokirmak *et al.*, Rev. Sci. Instrum. **69**, 3410 (1998).
[15] C. Dembowski *et al.*, Phys. Rev. Lett. **84**, 867 (2000).
[16] N. Savytskyy, O. Hul, and L. Sirko, Phys. Rev. E **70**, 056209 (2004).
[17] C. Dembowski *et al.*, Phys. Rev. E **60**, 3942 (1999).
[18] J. Stein and H.-J. Stöckmann, Phys. Rev. Lett. **68**, 2867 (1992).
[19] W. H. Press *et al.*, *Numerical Recipes in C* (Cambridge University Press, Cambridge, England, 1992).
[20] E. Bogomolny and C. Schmit, Nonlinearity **16**, 2035 (2003).